

1 **SARS-CoV-2 causes brain inflammation and induces Lewy body formation in macaques**

2
3 Ingrid H.C.H.M. Philippens^{1,*†}, Kinga P. Böszörményi^{1†}, Jacqueline A. Wubben¹, Zahra C.
4 Fagrouch¹, Nikki van Driel¹, Amber Q. Mayenburg¹, Diana Lozovagia¹, Eva Roos², Bernadette
5 Schurink², Marianna Bugiani², Ronald E. Bontrop^{1,3}, Jinte Middeldorp¹, Willy M. Bogers¹, Lioe-Fee
6 de Geus-Oei^{5,6}, Jan A.M. Langermans^{1,4}, Marieke A. Stammes^{1‡}, Babs E. Verstrepen^{1‡}, Ernst J.
7 Verschoor^{1‡}

8
9 ¹ Biomedical Primate Research Centre (BPRC), Lange Kleiweg 161, 2288GJ Rijswijk, The
10 Netherlands

11 ² Department of Pathology, Amsterdam UMC, De Boelelaan 1117, 1081HV Amsterdam, The
12 Netherlands

13 ³ Department of Biology, Theoretical Biology and Bioinformatics, Utrecht University, Padualaan
14 8, Utrecht, The Netherlands

15 ⁴ Department Population Health Sciences, Division of Animals in Science and Society, Faculty of
16 Veterinary Medicine, Utrecht University, Yalelaan 1, 3584CL Utrecht, The Netherlands

17 ⁵ Department of Radiology, Leiden University Medical Center, Albinusdreef 2, 2333ZA Leiden,
18 The Netherlands

19 ⁶ Biomedical Photonic Imaging Group, University of Twente, Drienerlolaan 5, 7522ND Enschede,
20 The Netherlands

21
22 † These authors contributed equally

23 ‡ These authors jointly supervised this work

24 *Corresponding author. E-mail: philippens@bprc.nl

25
26
27
28 **Keywords:** SARS-CoV-2; macaques; brain inflammation; Lewy body formation; neuropathology;
29 PET-CT

30
31

32
33
34
35
36
37
38
39
40
41
42
43
44
45
46
47
48
49
50
51

Abstract:

SARS-CoV-2 may cause acute respiratory disease, but the infection can also initiate neurological symptoms. Here we show that SARS-CoV-2 infection causes brain inflammation in the macaque model. An increased metabolic activity in the pituitary gland of two macaques was observed by longitudinal positron emission tomography-computed tomography (PET-CT). Post-mortem analysis demonstrated infiltration of T-cells and activated microglia in the brain, and viral RNA was detected in brain tissues from one animal. We observed Lewy bodies in brains of all rhesus macaques. These data emphasize the virus' capability to induce neuropathology in this nonhuman primate model for SARS-CoV-2 infection. As in humans Lewy body formation is an indication for the development of Parkinson's disease, this data represents a warning for potential long-term neurological effects after SARS-CoV-2 infection.

One-Sentence Summar:

SARS-CoV-2 causes brain inflammation and Lewy bodies, a hallmark for Parkinson, after an asymptomatic infection in macaques.

52 **Report**

53 Severe acute respiratory syndrome coronavirus 2 (SARS-CoV-2) causes a multi-system
54 inflammatory disease syndrome, COVID-19 (1). Although SARS-CoV-2 predominantly affects
55 the respiratory organs, over 30% of the hospitalized COVID-19 patients also suffer from
56 neurological manifestations, including loss of smell or taste, delirium, diminished consciousness,
57 epilepsy, and psychosis (2-5). Besides these general neurological symptoms, some patients
58 additionally endure Parkinsonism (6-8). The mechanisms behind this process are poorly
59 understood. Neurological symptoms may be triggered by infection of the brain tissue, or indirectly,
60 via virus-induced immune cell activation (9). In humans a direct link between brain inflammation
61 and the presence of SARS-CoV-2 RNA has not yet been established (10), and thus, formal proof
62 that central nervous system (CNS)-related symptoms of COVID-19 are directly caused by the
63 infection, or indirectly due to overactivation of the immune system, is lacking. Additionally, the
64 long-term effects on the CNS after a mild to moderate SARS-CoV-2 infection, likely the vast
65 majority of human cases, are unknown, and post-mortem brain samples from these individuals are
66 not expected to become available for research in the near future. Controlled infection studies in a
67 standardized experimental setting are crucial to investigate SARS-CoV-2-induced brain pathology
68 (11). To address this issue, a study was performed in two macaques species, rhesus macaques
69 (*Macaca mulatta*) and cynomolgus macaques (*Macaca fascicularis*) (Table 1), both well-accepted
70 animal models for COVID-19 (12). Four male rhesus and four male cynomolgus macaques were
71 inoculated with 10^6 TCID₅₀ of SARS-CoV-2 strain BetaCoV/BavPat1/2020 via a combined
72 intratracheal and intranasal route (13, 14). Following infection, SARS-CoV-2 genomic material
73 was detected in tracheal and nasal swabs up to ten days, and based on clinical signs and thorax
74 CTs, all animals showed mild to moderate disease symptoms (13, 15). We initiated weekly ¹⁸F-FDG

75 PET-CTs of the animals' brains of all macaques when the virus became undetectable in nasal and
76 tracheal swabs. The uptake of tracer renders a marker for metabolic activity. Two of four
77 cynomolgus macaques (C1 and C2), displayed an increased uptake of ^{18}F -FDG in the pituitary gland
78 at multiple time points. In animal C1, an increased uptake of ^{18}F -FDG in the pituitary gland was
79 seen at days 30 and 36 post-infection (Fig. 1). In animal C2, increased metabolic activity was
80 already visible at day 8 and continued through day 35 when the final scan was obtained (Table S1).
81 In humans and macaques, the volume of the pituitary gland is small, and under physiological
82 conditions its metabolic activity is comparable to the background level of the entire brain (16, 17).
83 The ^{18}F -FDG uptake of the pituitary gland may even be underestimated due to the partial-volume-
84 effects that affect the emission signal recovery (16). Because pituitary gland tissue expresses
85 angiotensin-converting enzyme 2 (ACE2)(18), the increased ^{18}F -FDG uptake may be a direct effect
86 of the infection or an indirect effect due to either a (reversible) hypophysitis, or transient
87 hypothalamic-pituitary dysfunction. Yet, hypocortisolism has never been documented in patients
88 with active COVID-19 (19).

89 To further investigate the consequences of SARS-CoV-2-infection on macaque brain tissue, the
90 animals were euthanized 5-6 weeks after experimental infection. Sections of the whole brain were
91 systematically collected for further examination. As several regions of the brain express the SARS-
92 CoV-2 receptor ACE2, and inflammation was found in the human brain (10, 20, 21), we used
93 various immunological markers for innate and adaptive immune activation to investigate for signs
94 of immune activation, and also explored the localization of virus particles (Fig. 2 and Table 2).
95 Viral RNA was detected by real-time quantitative polymerase chain reaction (RT-qPCR) in
96 multiple brain areas of the right hemisphere of cynomolgus macaque C3 (Fig. 2). More precisely,
97 cerebellum (1.48×10^5 RNA genome equivalents (GE)/gram), medial motor cortex (2.09×10^5

98 GE/gram), sensory cortex (2.07×10^5 GE/gram) and frontal basal cortex (8.29×10^4 GE/gram), as well
99 as hippocampus (1.24×10^5 GE/gram), hypothalamus (1.05×10^6 GE/gram), and globus pallidus
100 (5.45×10^4 GE/gram) all tested positive in the RT-qPCR. No viral RNA was detected in samples
101 collected from the pituitary gland or olfactory bulb, substantia nigra, medulla oblongata, pons,
102 nucleus caudatus, and putamen. Subgenomic viral RNA analysis did not show evidence for active
103 virus replication in the brains at the time-point of euthanasia. Additionally, SARS-CoV-2 antigen
104 was not detectable by immunohistochemistry the brains of all macaques.

105 The brains of all SARS-CoV-2-infected macaques showed evidence of inflammation. Presence of
106 T-cells was visualized by CD3 staining in intraparenchymal brain tissue, suggesting the infiltration
107 of T-cells that passed the blood-brain barrier after SARS-CoV-2 infection (Fig.3A, top panel).
108 Additionally, activation of microglia cells in different areas of the brain, including the olfactory
109 bulb and pituitary gland, was confirmed by Mamu-DR staining (upregulation of MHC class II
110 expression) (Fig. 3A, middle panel). However, nodule formation, which is a measure for severity
111 of activation, was rarely present (Table 2). No B-lymphocytic infiltration was found as evidenced
112 by lack of CD20 staining (not shown). Hematoxylin and eosin (HE) staining did not show any
113 abnormalities in the brain tissue of the virus-exposed macaques, including the absence of
114 ischemic/necrotic lesions. For comparison, post-mortem brain tissues from two healthy, age-
115 matched macaques of each species were used as controls (Table 1), none of the four control animals
116 displayed obvious signs of immune activation (T-cells and microglia) were observed.

117 Brain tissues were screened for α -synuclein deposits, known as Lewy bodies, by
118 immunohistochemistry. In humans, Lewy body formation is linked to the development of
119 Parkinson's disease or Lewy body dementia (22, 23). It has been hypothesized that certain

120 neurotropic viruses, including MERS and SARS coronaviruses, can trigger formation of Lewy
121 bodies and cause Parkinsonism (24-29).

122 The formation of intracellular Lewy bodies was clearly shown in the midbrain region of the caudate
123 nucleus of all infected rhesus macaques (Table 2, Fig. 3B), and in one aged cynomolgus macaque
124 (C4), while Lewy bodies were absent in the brains of all four control animals. The data provide
125 evidence for SARS-CoV-2-driven inflammation in the brain of macaques. In humans,
126 neuropathology has been described in moribund COVID-19 patients, but we report of SARS-CoV-
127 2-related brain involvement in macaques without displaying overt clinical signs. In general,
128 macaque models for SARS-CoV-2 infection typically represent mild to moderate COVID-19
129 symptoms on the CT scan, as compared to humans (12, 14, 30). Detection of viral RNA in the brain
130 of an animal demonstrates the virus' neuroinvasive capability. This matches a recent study
131 describing neuroinvasion in mouse brains and in human brain organoids (31).

132 How exactly SARS-CoV-2 caused widespread brain inflammation and induced Lewy body
133 formation remains unknown. Viruses can enter the brain via different pathways. In this study,
134 infiltration of T-cells was found perivascular and in the brain parenchyma, which indicates that the
135 blood-brain barrier integrity may have been disturbed, offering the virus the opportunity to enter
136 the brain. Alternatively, we hypothesize that SARS-CoV-2 gained access to the brain via neuronal
137 pathways, such as the retrograde and anterograde neuronal transport through infected motor or
138 sensory neurons (32), and can have entered the pituitary gland via binding to the ACE2 receptor
139 protein expressed on its cell surfaces (18, 33). Such neural connection also exists between the
140 olfactory bulb and the nasal mucosa (34), and the loss of taste and smell, a characteristic of COVID-
141 19, can thus be explained by nasal infection and subsequent inflammation in the olfactory bulb.
142 Such a scenario is in line with the finding that in all the SARS-CoV-2-exposed macaques, immune

143 system activation in the olfactory bulb was evidenced by the presence of T-cells and/or activated
144 microglia.

145 Neuronal transport can also explain why some COVID-19 patients develop Parkinson's disease-
146 like symptoms. Viruses can also, via retrograde transport in parasympathic motor neurons of the
147 nervus vagus to the medulla, pons, and midbrain, reach the substantia nigra in the midbrain (26,
148 35). Notably, the α -synuclein inclusions were found in the ventral midbrain region of the animals.
149 In humans, these inclusions of accumulated misfolded proteins are associated with Parkinson's
150 disease or Lewy body dementia (36).

151 There is a growing concern that symptomatic COVID-19 patients may suffer from long-term
152 consequences (9, 37). In this light the finding of Lewy bodies in brains of infected macaques
153 without overt clinical signs is intriguing. They are considered a hallmark for the development of
154 Parkinson's disease, or Lewy body dementia. More confirmation is required, but the observations
155 in the translational macaque models for COVID-19 (12-14, 38, 39) can be regarded as a serious
156 warning as they may be predictive for COVID-19-related dementia cases in humans in the future,
157 even after an asymptomatic infection or mild disease process.

158

159 **References**

- 160 1. V. Coronaviridae Study Group of the International Committee on Taxonomy of, The
161 species Severe acute respiratory syndrome-related coronavirus: classifying 2019-nCoV
162 and naming it SARS-CoV-2. *Nat Microbiol* **5**, 536-544 (2020).
- 163 2. L. Mao, H. Jin, M. Wang, Y. Hu, S. Chen, Q. He, J. Chang, C. Hong, Y. Zhou, D. Wang,
164 X. Miao, Y. Li, B. Hu, Neurologic Manifestations of Hospitalized Patients With
165 Coronavirus Disease 2019 in Wuhan, China. *JAMA Neurol* **77**, 683-690 (2020).
- 166 3. R. W. Paterson, R. L. Brown, L. Benjamin, R. Nortley, S. Wiethoff, T. Bharucha, D. L.
167 Jayaseelan, G. Kumar, R. E. Raftopoulos, L. Zambreau, V. Vivekanandam, A. Khoo, R.
168 Geraldine, K. Chinthapalli, E. Boyd, H. Tuzlali, G. Price, G. Christofi, J. Morrow, P.
169 McNamara, B. McLoughlin, S. T. Lim, P. R. Mehta, V. Levee, S. Keddie, W. Yong, S. A.
170 Trip, A. J. M. Foulkes, G. Hotton, T. D. Miller, A. D. Everitt, C. Carswell, N. W. S.
171 Davies, M. Yoong, D. Attwell, J. Sreedharan, E. Silber, J. M. Schott, A. Chandratheva, R.
172 J. Perry, R. Simister, A. Checkley, N. Longley, S. F. Farmer, F. Carletti, C. Houlihan, M.

- 173 Thom, M. P. Lunn, J. Spillane, R. Howard, A. Vincent, D. J. Werring, C. Hoskote, H. R.
174 Jager, H. Manji, M. S. Zandi, U. C. L. Q. S. N. H. f. Neurology, C.-S. G. Neurosurgery,
175 The emerging spectrum of COVID-19 neurology: clinical, radiological and laboratory
176 findings. *Brain*, (2020).
- 177 4. M. Fotuhi, A. Mian, S. Meysami, C. A. Raji, Neurobiology of COVID-19. *J Alzheimers*
178 *Dis* **76**, 3-19 (2020).
- 179 5. A. Giacomelli, L. Pezzati, F. Conti, D. Bernacchia, M. Siano, L. Oreni, S. Rusconi, C.
180 Gervasoni, A. L. Ridolfo, G. Rizzardini, S. Antinori, M. Galli, Self-reported Olfactory
181 and Taste Disorders in Patients With Severe Acute Respiratory Coronavirus 2 Infection:
182 A Cross-sectional Study. *Clin Infect Dis* **71**, 889-890 (2020).
- 183 6. M. E. Cohen, R. Eichel, B. Steiner-Birmanns, A. Janah, M. Ioshpa, R. Bar-Shalom, J. J.
184 Paul, H. Gaber, V. Skrahina, N. M. Bornstein, G. Yahalom, A case of probable
185 Parkinson's disease after SARS-CoV-2 infection. *Lancet Neurol* **19**, 804-805 (2020).
- 186 7. I. Faber, P. R. P. Brandao, F. Menegatti, D. D. de Carvalho Bispo, F. B. Maluf, F.
187 Cardoso, Coronavirus Disease 2019 and Parkinsonism: A Non-post-encephalitic Case.
188 *Mov Disord* **35**, 1721-1722 (2020).
- 189 8. A. Mendez-Guerrero, M. I. Laespada-Garcia, A. Gomez-Grande, M. Ruiz-Ortiz, V. A.
190 Blanco-Palmero, F. J. Azcarate-Diaz, P. Rabano-Suarez, E. Alvarez-Torres, C. P. de
191 Fuenmayor-Fernandez de la Hoz, D. Vega Perez, R. Rodriguez-Montalban, A. Perez-
192 Rivilla, J. Sayas Catalan, A. Ramos-Gonzalez, J. Gonzalez de la Aleja, Acute
193 hypokinetic-rigid syndrome following SARS-CoV-2 infection. *Neurology* **95**, e2109-
194 e2118 (2020).
- 195 9. M. T. Heneka, D. Golenbock, E. Latz, D. Morgan, R. Brown, Immediate and long-term
196 consequences of COVID-19 infections for the development of neurological disease.
197 *Alzheimers Res Ther* **12**, 69 (2020).
- 198 10. B. Schurink, E. Roos, T. Radonic, E. Barbe, C. S. C. Bouman, H. H. de Boer, G. J. de
199 Bree, E. B. Bulle, E. M. Aronica, S. Florquin, J. Fronczek, L. M. A. Heunks, M. D. de
200 Jong, L. Guo, R. du Long, R. Lutter, P. C. G. Molenaar, E. A. Neefjes-Borst, H. W. M.
201 Niessen, C. J. M. van Noesel, J. Roelofs, E. J. Snijder, E. C. Soer, J. Verheij, A. P. J.
202 Vlaar, W. Vos, N. N. van der Wel, A. C. van der Wal, P. van der Valk, M. Bugiani, Viral
203 presence and immunopathology in patients with lethal COVID-19: a prospective autopsy
204 cohort study. *Lancet Microbe* **1**, e290-e299 (2020).
- 205 11. S. Natoli, V. Oliveira, P. Calabresi, L. F. Maia, A. Pisani, Does SARS-Cov-2 invade the
206 brain? Translational lessons from animal models. *Eur J Neurol* **27**, 1764-1773 (2020).
- 207 12. C. Munoz-Fontela, W. E. Dowling, S. G. P. Funnell, P. S. Gsell, A. X. Riveros-Balta, R.
208 A. Albrecht, H. Andersen, R. S. Baric, M. W. Carroll, M. Cavaleri, C. Qin, I. Crozier, K.
209 Dallmeier, L. de Waal, E. de Wit, L. Delang, E. Dohm, W. P. Duprex, D. Falzarano, C. L.
210 Finch, M. B. Frieman, B. S. Graham, L. E. Gralinski, K. Guilfoyle, B. L. Haagmans, G.
211 A. Hamilton, A. L. Hartman, S. Herfst, S. J. F. Kaptein, W. B. Klimstra, I. Knezevic, P.
212 R. Krause, J. H. Kuhn, R. Le Grand, M. G. Lewis, W. C. Liu, P. Maisonnasse, A. K.
213 McElroy, V. Munster, N. Oreshkova, A. L. Rasmussen, J. Rocha-Pereira, B. Rockx, E.
214 Rodriguez, T. F. Rogers, F. J. Salguero, M. Schotsaert, K. J. Stittelaar, H. J. Thibaut, C. T.
215 Tseng, J. Vergara-Alert, M. Beer, T. Brasel, J. F. W. Chan, A. Garcia-Sastre, J. Neyts, S.
216 Perlman, D. S. Reed, J. A. Richt, C. J. Roy, J. Segales, S. S. Vasan, A. M. Henao-
217 Restrepo, D. H. Barouch, Animal models for COVID-19. *Nature* **586**, 509-515 (2020).

- 218 13. K. P. Böszörményi, M. A. Stammes, Z. C. Fagrouch, G. Kiemenyi-Kayere, H. Niphuis, D.
219 Mortier, N. van Driel, I. Nieuwenhuis, E. Zuiderwijk-Sick, L. Meijer, P. Mooij, E. J.
220 Remarque, G. Koopman, A. C. R. Hoste, P. Sastre, B. L. Haagmans, R. E. Bontrop, J. A.
221 M. Langermans, W. M. Bogers, E. J. Verschoor, B. E. Verstrepen, Comparison of SARS-
222 CoV-2 infection in two non-human primate species: rhesus and cynomolgus macaques.
223 *bioRxiv*, 11.05.369413 (2020).
- 224 14. B. Rockx, T. Kuiken, S. Herfst, T. Bestebroer, M. M. Lamers, B. B. Oude Munnink, D. de
225 Meulder, G. van Amerongen, J. van den Brand, N. M. A. Okba, D. Schipper, P. van Run,
226 L. Leijten, R. Sikkema, E. Verschoor, B. Verstrepen, W. Bogers, J. Langermans, C.
227 Drosten, M. Fentener van Vlissingen, R. Fouchier, R. de Swart, M. Koopmans, B. L.
228 Haagmans, Comparative pathogenesis of COVID-19, MERS, and SARS in a nonhuman
229 primate model. *Science* **368**, 1012-1015 (2020).
- 230 15. F. Pan, T. Ye, P. Sun, S. Gui, B. Liang, L. Li, D. Zheng, J. Wang, R. L. Hesketh, L. Yang,
231 C. Zheng, Time Course of Lung Changes at Chest CT during Recovery from Coronavirus
232 Disease 2019 (COVID-19). *Radiology* **295**, 715-721 (2020).
- 233 16. M. Meyer, G. Allenbach, M. Nicod Lalonde, N. Schaefer, J. O. Prior, S. Gnesin,
234 Increased (18)F-FDG signal recovery from small physiological structures in digital
235 PET/CT and application to the pituitary gland. *Sci Rep* **10**, 368 (2020).
- 236 17. S. Goutal, N. Tournier, M. Guillermier, N. Van Camp, O. Barret, M. Gaudin, M.
237 Bottlaender, P. Hantraye, S. Lavis, Comparative test-retest variability of outcome
238 parameters derived from brain [18F]FDG PET studies in non-human primates. *PLoS One*
239 **15**, e0240228 (2020).
- 240 18. R. Pal, M. Banerjee, COVID-19 and the endocrine system: exploring the unexplored. *J*
241 *Endocrinol Invest* **43**, 1027-1031 (2020).
- 242 19. R. Pal, COVID-19, hypothalamo-pituitary-adrenal axis and clinical implications.
243 *Endocrine*, (2020).
- 244 20. I. Hamming, W. Timens, M. L. Bulthuis, A. T. Lely, G. Navis, H. van Goor, Tissue
245 distribution of ACE2 protein, the functional receptor for SARS coronavirus. A first step in
246 understanding SARS pathogenesis. *J Pathol* **203**, 631-637 (2004).
- 247 21. M. Hoffmann, H. Kleine-Weber, S. Schroeder, N. Kruger, T. Herrler, S. Erichsen, T. S.
248 Schiergens, G. Herrler, N. H. Wu, A. Nitsche, M. A. Muller, C. Drosten, S. Pohlmann,
249 SARS-CoV-2 Cell Entry Depends on ACE2 and TMPRSS2 and Is Blocked by a
250 Clinically Proven Protease Inhibitor. *Cell* **181**, 271-280 e278 (2020).
- 251 22. Z. Walker, K. L. Possin, B. F. Boeve, D. Aarsland, Lewy body dementias. *Lancet* **386**,
252 1683-1697 (2015).
- 253 23. M. Sezgin, B. Bilgic, S. Tinaz, M. Emre, Parkinson's Disease Dementia and Lewy Body
254 Disease. *Semin Neurol* **39**, 274-282 (2019).
- 255 24. T. Yamada, Viral etiology of Parkinson's disease: Focus on influenza A virus.
256 *Parkinsonism Relat Disord* **2**, 113-121 (1996).
- 257 25. R. L. Doty, The olfactory vector hypothesis of neurodegenerative disease: is it viable?
258 *Ann Neurol* **63**, 7-15 (2008).
- 259 26. I. Mori, Viremic attack explains the dual-hit theory of Parkinson's disease. *Med*
260 *Hypotheses* **101**, 33-36 (2017).
- 261 27. E. M. Gatto, J. Fernandez Boccazzi, COVID-19 and neurodegeneration: what can we
262 learn from the past? *Eur J Neurol* **27**, e45 (2020).

- 263 28. A. Y. Vittor, M. Long, P. Chakrabarty, L. Aycock, V. Kollu, S. T. DeKosky, West Nile
264 Virus-Induced Neurologic Sequelae-Relationship to Neurodegenerative Cascades and
265 Dementias. *Curr Trop Med Rep* **7**, 25-36 (2020).
- 266 29. S. Ait Wahmane, A. Achbani, Z. Ouhaz, M. Elatiqi, A. Belmouden, M. Nejmeddine, The
267 Possible Protective Role of alpha-Synuclein Against Severe Acute Respiratory Syndrome
268 Coronavirus 2 Infections in Patients With Parkinson's Disease. *Mov Disord* **35**, 1293-
269 1294 (2020).
- 270 30. D. K. Singh, B. Singh, S. R. Ganatra, M. Gazi, J. Cole, R. Thippeshappa, K. J. Alfson, E.
271 Clemmons, O. Gonzalez, R. Escobedo, T. H. Lee, A. Chatterjee, Y. Goetz-Gazi, R.
272 Sharan, M. Gough, C. Alvarez, A. Blakley, J. Ferdin, C. Bartley, H. Staples, L. Parodi, J.
273 Callery, A. Mannino, B. Klaffke, P. Escareno, R. N. Platt, 2nd, V. Hodara, J. Scordo, S.
274 Gautam, A. G. Vilanova, A. Olmo-Fontanez, A. Schami, A. Oyejide, D. K. Ajithdoss, R.
275 Copin, A. Baum, C. Kyratsous, X. Alvarez, M. Ahmed, B. Rosa, A. Goodroe, J. Dutton,
276 S. Hall-Ursone, P. A. Frost, A. K. Voges, C. N. Ross, K. Sayers, C. Chen, C. Hallam, S.
277 A. Khader, M. Mitreva, T. J. C. Anderson, L. Martinez-Sobrido, J. L. Patterson, J. Turner,
278 J. B. Torrelles, E. J. Dick, Jr., K. Brasky, L. S. Schlesinger, L. D. Giavedoni, R. Carrion,
279 Jr., D. Kaushal, Responses to acute infection with SARS-CoV-2 in the lungs of rhesus
280 macaques, baboons and marmosets. *Nat Microbiol* **6**, 73-86 (2021).
- 281 31. E. Song, C. Zhang, B. Israelow, A. Lu-Culligan, A. V. Prado, S. Skriabine, P. Lu, O. E.
282 Weizman, F. Liu, Y. Dai, K. Szigeti-Buck, Y. Yasumoto, G. Wang, C. Castaldi, J. Heltke,
283 E. Ng, J. Wheeler, M. M. Alfajaro, E. Levavasseur, B. Fontes, N. G. Ravindra, D. Van
284 Dijk, S. Mane, M. Gunel, A. Ring, S. A. J. Kazmi, K. Zhang, C. B. Wilen, T. L. Horvath,
285 I. Plu, S. Haik, J. L. Thomas, A. Louvi, S. F. Farhadian, A. Huttner, D. Seilhean, N.
286 Renier, K. Bilguvar, A. Iwasaki, Neuroinvasion of SARS-CoV-2 in human and mouse
287 brain. *J Exp Med* **218**, (2021).
- 288 32. P. A. Swanson, 2nd, D. B. McGavern, Viral diseases of the central nervous system. *Curr*
289 *Opin Virol* **11**, 44-54 (2015).
- 290 33. E. Lazartigues, M. M. F. Qadir, F. Mauvais-Jarvis, Endocrine Significance of SARS-
291 CoV-2's Reliance on ACE2. *Endocrinology* **161**, (2020).
- 292 34. J. Meinhardt, J. Radke, C. Dittmayer, J. Franz, C. Thomas, R. Mothes, M. Laue, J.
293 Schneider, S. Brünink, S. Greuel, M. Lehmann, O. Hassan, T. Aschman, E. Schumann, R.
294 L. Chua, C. Conrad, R. Eils, W. Stenzel, M. Windgassen, L. Röbler, H.-H. Goebel, H. R.
295 Gelderblom, H. Martin, A. Nitsche, W. J. Schulz-Schaeffer, S. Hakrrouch, M. S. Winkler,
296 B. Tampe, F. Scheibe, P. Körtvélyessy, D. Reinhold, B. Siegmund, A. A. Köhl, S.
297 Elezkurtaj, D. Horst, L. Oesterhelweg, M. Tsokos, B. Ingold-Heppner, C. Stadelmann, C.
298 Drosten, V. M. Corman, H. Radbruch, F. L. Heppner, Olfactory transmucosal SARS-
299 CoV-2 invasion as a port of central nervous system entry in individuals with COVID-19.
300 *Nature Neuroscience*, (2020).
- 301 35. C. H. Hawkes, K. Del Tredici, H. Braak, Parkinson's disease: a dual-hit hypothesis.
302 *Neuropathol Appl Neurobiol* **33**, 599-614 (2007).
- 303 36. J. P. Taylor, J. Hardy, K. H. Fischbeck, Toxic proteins in neurodegenerative disease.
304 *Science* **296**, 1991-1995 (2002).
- 305 37. M. Marshall, The lasting misery of coronavirus long-haulers. *Nature* **585**, 339-341
306 (2020).
- 307 38. H. Zheng, H. Li, L. Guo, Y. Liang, J. Li, X. Wang, Y. Hu, L. Wang, Y. Liao, F. Yang, Y.
308 Li, S. Fan, D. Li, P. Cui, Q. Wang, H. Shi, Y. Chen, Z. Yang, J. Yang, D. Shen, W. Cun,

- 309 X. Zhou, X. Dong, Y. Wang, Y. Chen, Q. Dai, W. Jin, Z. He, Q. Li, L. Liu, Virulence and
310 pathogenesis of SARS-CoV-2 infection in rhesus macaques: A nonhuman primate model
311 of COVID-19 progression. *PLoS Pathog* **16**, e1008949 (2020).
- 312 39. V. J. Munster, F. Feldmann, B. N. Williamson, N. van Doremalen, L. Perez-Perez, J.
313 Schulz, K. Meade-White, A. Okumura, J. Callison, B. Brumbaugh, V. A. Avanzato, R.
314 Rosenke, P. W. Hanley, G. Saturday, D. Scott, E. R. Fischer, E. de Wit, Respiratory
315 disease in rhesus macaques inoculated with SARS-CoV-2. *Nature* **585**, 268-272 (2020).
- 316 40. M. A. Stammes, J. Bakker, R. A. W. Vervenne, D. G. M. Zijlmans, L. van Geest, M. P.
317 M. Vierboom, J. A. M. Langermans, F. A. W. Verreck, Recommendations for
318 Standardizing Thorax PET-CT in Non-Human Primates by Recent Experience from
319 Macaque Studies. *Animals* **11**, 204 (2021).
- 320 41. V. M. Corman, O. Landt, M. Kaiser, R. Molenkamp, A. Meijer, D. K. Chu, T. Bleicker, S.
321 Brunink, J. Schneider, M. L. Schmidt, D. G. Mulders, B. L. Haagmans, B. van der Veer,
322 S. van den Brink, L. Wijsman, G. Goderski, J. L. Romette, J. Ellis, M. Zambon, M. Peiris,
323 H. Goossens, C. Reusken, M. P. Koopmans, C. Drosten, Detection of 2019 novel
324 coronavirus (2019-nCoV) by real-time RT-PCR. *Euro Surveill* **25**, (2020).
- 325 42. R. Wolfel, V. M. Corman, W. Guggemos, M. Seilmaier, S. Zange, M. A. Muller, D.
326 Niemeyer, T. C. Jones, P. Vollmar, C. Rothe, M. Hoelscher, T. Bleicker, S. Brunink, J.
327 Schneider, R. Ehmann, K. Zwirgmaier, C. Drosten, C. Wendtner, Virological assessment
328 of hospitalized patients with COVID-2019. *Nature* **581**, 465-469 (2020).
- 329 43. G. Paxinos, X. F. Huang, M. Petrides, A. Toga, *The Rhesus Monkey Brain: in Stereotaxic*
330 *Coordinates*. (Elsevier Science Publishing Co Inc, San Diego, Ca., ed. 2nd, 2008), pp.
331 416.
332

333 **Acknowledgements**

334 We want to thank Francisca van Hassel for assistance with editing of figures, Yolanda Kap for
335 reviewing the manuscript, Wim Vos for the excellent histology, and the Animal Science
336 Department of the BPRC, the veterinarians and animal caretakers for all the experimental support.

338 **Funding**

339 This study was supported by funding from the Biomedical Primate Research Centre. KPB was
340 supported by the European Union's Marie Skłodowska-Curie Innovative Training Network
341 HONOURS; grant agreement no. 721367.

343 **Author contributions**

344 Conceptualization: IHCHMP, EJV, MAS, BEV

345 Data curation: MAS, BEV, IHCHMP

346 Formal Analysis: MAS, IHCHMP, BEV

347 Funding acquisition: EJV

348 Investigation: JAW, ZCF, NvD, AQM, DL

349 Methodology: MAS, MB, BS, IHCHMP

350 Project administration: EJV, BEV

351 Resources: REB

352 Supervision: IHCHMP, MAS, BEV, EJV

353 Validation: MB, ER, L-FG-O,

354 Writing – original draft: IHCHMP, KPB

355 Writing – review & editing: MAS, EJV, BEV, JAML, REB, JM, WMB,

356

357 **Competing interests:**

358 The authors declare that they have no competing interests.

359

360 **Data and materials availability:**

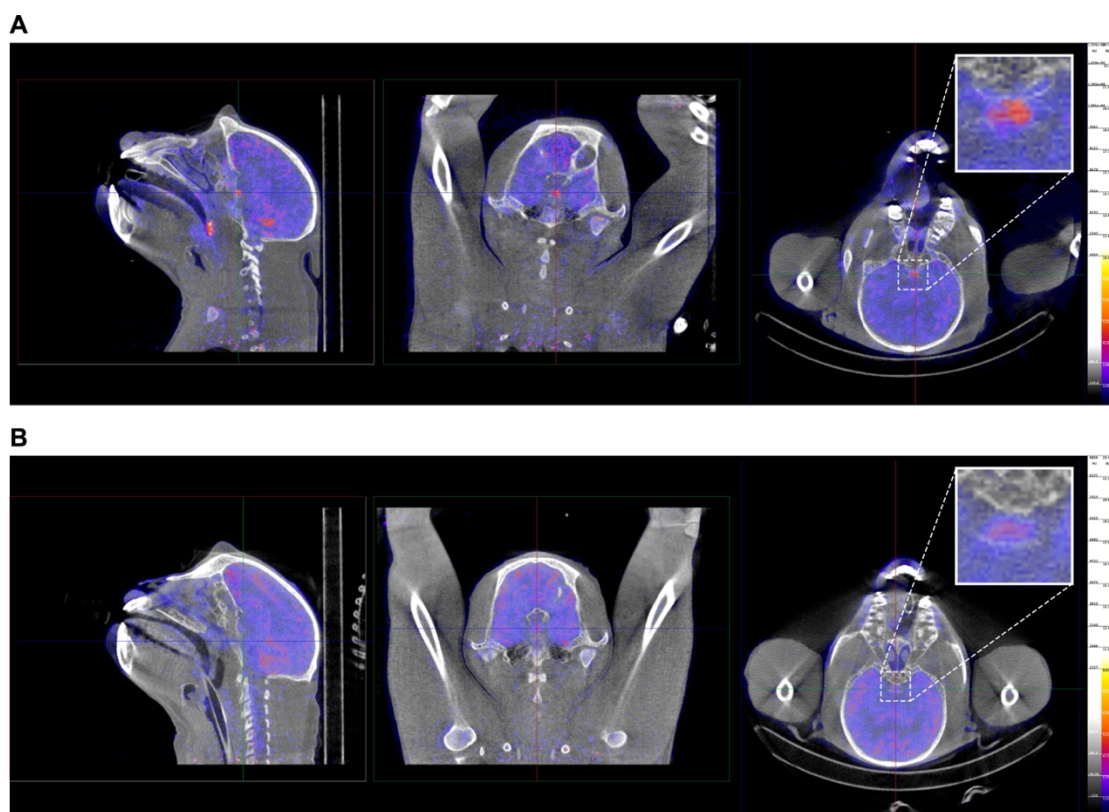
361 All data are available in the main text or the supplementary materials. Correspondence and request

362 for materials should be addressed to IHCHMP (philippens@bprc.nl).

363 **Table 1: Animals featuring in this study**

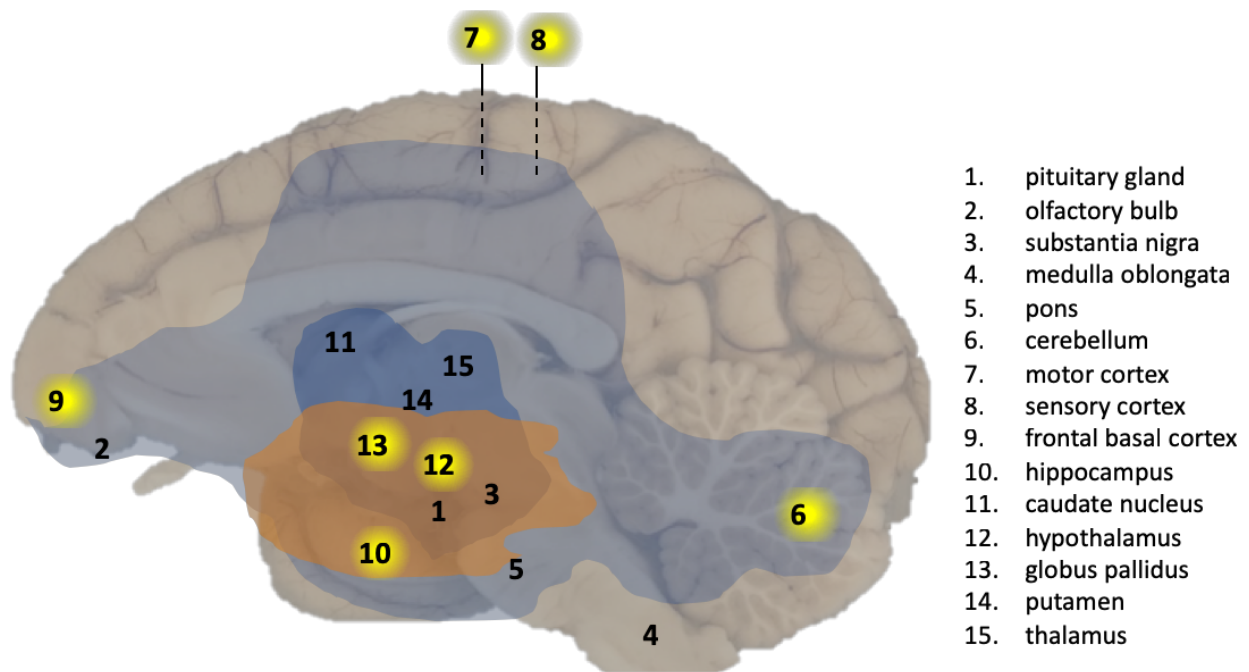
| Macaque species | Monkey ID | Infected Y/N | Age (Year) | Body weight ^a (kg) | Sex M/F |
|-----------------|------------|--------------|------------|-------------------------------|---------|
| Rhesus | R1 | Y | 6 | 8.2 | M |
| Rhesus | R2 | Y | 5 | 7.9 | M |
| Rhesus | R3 | Y | 5 | 7.8 | M |
| Rhesus | R4 | Y | 5 | 8.7 | M |
| Rhesus | control R5 | N | 5 | 8.5 | M |
| Rhesus | control R6 | N | 6 | 5.1 | F |
| Cynomolgus | C1 | Y | 4 | 5.7 | M |
| Cynomolgus | C2 | Y | 4 | 3.3 | M |
| Cynomolgus | C3 | Y | 4 | 4.9 | M |
| Cynomolgus | C4 | Y | 16 | 9.7 | M |
| Cynomolgus | control C5 | N | 5 | 5.3 | M |
| Cynomolgus | control C6 | N | 7 | 5.1 | M |

364 ^aat start of study



365
366 **Fig. 1. ^{18}F -FDG PET-CT image of a SARS-CoV-2 infected cynomolgus macaque (C1).**
367 Representative images of cynomolgus macaque C1 (A) on day 29, and a healthy control animal
368 (B) are shown. The pituitary gland is indicated by the cross-hairs in all three directions and is boxed
369 (right pictures). Similar window-level settings are applied for all sections. The pituitary gland-brain
370 ratio of animal C1 was calculated with both the mean and peak standard uptake value (SUV); for
371 the SUV_{mean} this ratio was 1.9, and for the SUV_{peak} 1.3. The average values calculated from a group of
372 non-infected control animals (n=6) were 1.1 (std 0.3) for the SUV_{mean} , and 0.6 (std 0.1) for the SUV_{peak}
373 ratio. The uptake values of the brain, defined as background, were similar with SUV_{mean} values of
374 2.2 and 1.9 for the SARS-CoV-2-infected animals and the non-infected controls, respectively. After
375 the relevant corrections for attenuation, scatter and decay, our results are indeed indicative for
376 pituitary hypermetabolism after SARS-CoV-2 infection in animals C1 and C2.

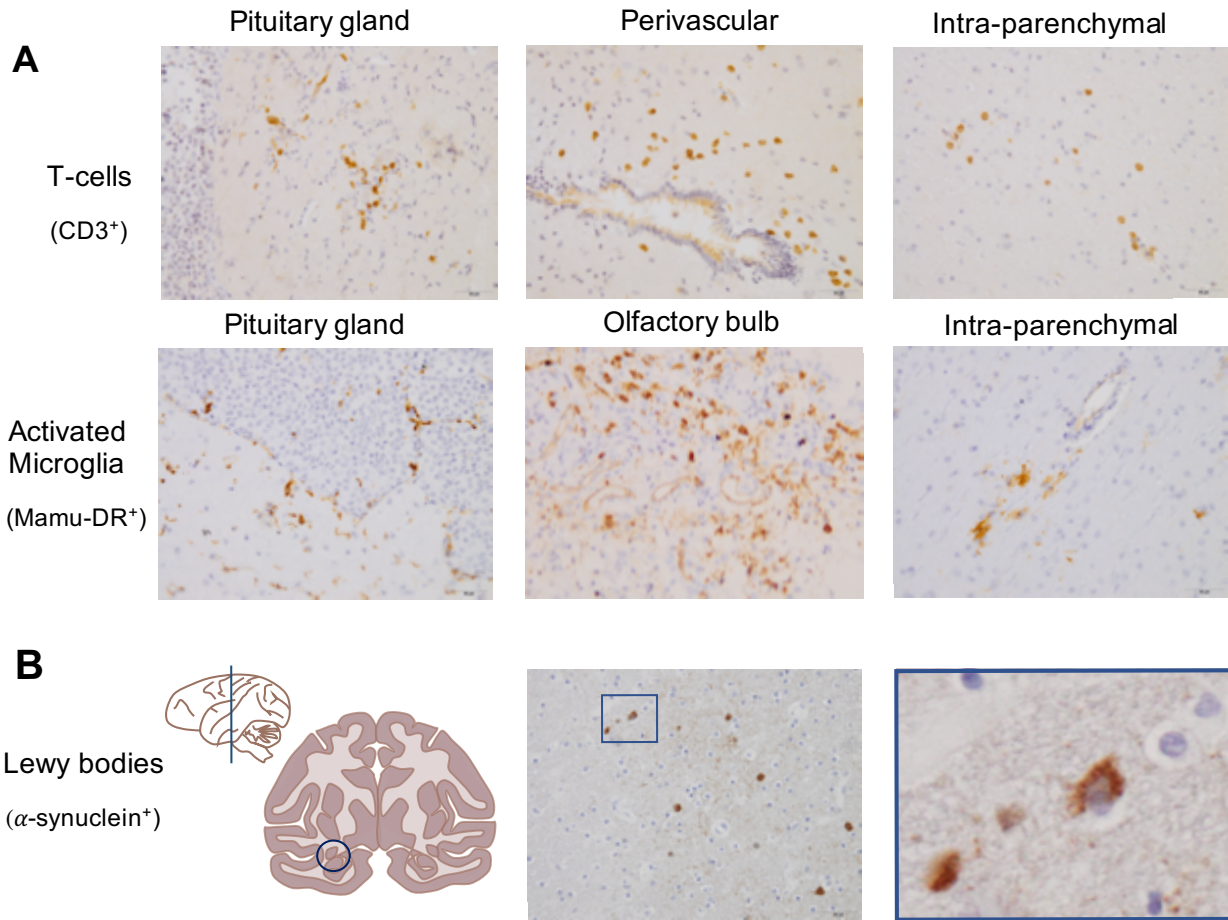
377



378

379 **Fig. 2. Overview of CNS effects by SARS-CoV-2 exposure in a macaque brain.** Presence of
380 viral RNA was investigated in multiple regions of the brain as indicated by the numbers. Viral
381 RNA-positive regions in cynomolgus macaque C3 are indicated by a yellow background. The
382 analysed brain regions are indicated with a number. Brain areas with T-cells (CD3+) and activated
383 microglia (Mamu-DR+) are shown in light blue (mild expression) and dark blue (moderate
384 expression), respectively. Brain areas with Lewy bodies (α -synuclein+) are shown in orange.

385



386

387 **Fig. 3. SARS-CoV-2 causes brain inflammation and Lewy body formation in brains of**

388 **macaques.** Immunohistochemical stainings of macaque brain tissues. **A**, top panel: T-cells (CD3⁺)

389 in the pituitary gland (left), perivascular (middle) and in the brain parenchyma (right) from a rhesus

390 macaque (20x). **A**, middle panel: activated microglia (Mamu-DR⁺) in the pituitary gland (left),

391 olfactory bulb (middle) and in the brain parenchyma (right) from a cynomolgus macaque (20x). **B**,

392 bottom panel: Lewy bodies (α-synuclein⁺) were found next to the hippocampus next to the caudate

393 nucleus indicated with a circle (left) in the coronal section of one hemisphere (anterior-posterior

394 0), presence of Lewy bodies in a SARS-CoV-2-infected rhesus macaque (20x) (middle), a

395 magnified image (40x) of the square in the left image (right).

396

397 **Table 2: Histological findings.**

| Marker | | Brain area | Rhesus | | | | Cynomolgus | | | | Controls | | | | |
|---------------------------------------|-------------------------------|-------------------------------------------------------------------------------------|--------|----|----|----|------------|----|----|----|----------|----|----|----|--|
| | | | R1 | R2 | R3 | R4 | C1 | C2 | C3 | C4 | R5 | R6 | C5 | C6 | |
| T-cells (CD3+) | intra-parenchymal | pituitary gland olfactory bulb front brain dorsal ventral cerebellum | | | | | | | | | | | | | |
| | perivascular | pituitary gland olfactory bulb front brain dorsal ventral cerebellum | | | | | | | | | | | | | |
| | nodules | pituitary gland olfactory bulb front brain dorsal ventral cerebellum | | | | | | | | | | | | | |
| | meninges | pituitary gland olfactory bulb front brain dorsal ventral cerebellum | | | | | | | | | | | | | |
| Activated microglia (Mamu-DR+) | presence | pituitary gland olfactory bulb front brain dorsal ventral cerebellum | | | | | | | | | | | | | |
| | morphology: ramified/amoeboid | pituitary gland olfactory bulb front brain dorsal ventral cerebellum | | | | | | | | | | | | | |
| | nodules | pituitary gland olfactory bulb front brain dorsal ventral cerebellum | | | | | | | | | | | | | |
| | meninges | pituitary gland olfactory bulb front brain dorsal ventral cerebellum | | | | | | | | | | | | | |
| Lewy bodies (α-synuclein+) | inclusions | ventral midbrain | | | | | | | | | | | | | |

398
399
400 Table 2 outlines the presence of 1) T-cells (CD3+ cells) in the brain tissue (intraparenchymal),
401 around blood vessels (perivascular), in group formation (nodules), or in the meninges, 2) activated

402 microglia (Mamu-DR+ cells) in different parts of the brain, the morphology as a measure for the
403 severity of activation (ramified or amoeboid), in group formation (nodules) or in the meninges, 3)
404 α -synuclein/Lewy bodies (α -synuclein + cells with inclusions) in the ventral midbrain region of
405 the caudate nucleus. The last column shows the absence of most of these markers in the control
406 animals. Light grey: mild observation; dark grey: moderate observation (including amoeboid
407 microglia cells); black: moderate to severe observation of these markers.

408

409

410

411

412

413

414

415

416

417

418

419

420

421

422

423

424

425

426

427

428

429

430

431 **Supplementary Materials for**

432

433 **SARS-CoV-2 causes brain inflammation and induces Lewy body formation in macaques**

434

435 Ingrid H.C.H.M. Philippens^{1,*†}, Kinga P. Böszörményi^{1†}, Jacqueline A. Wubben¹, Zahra C.
436 Fagrouch¹, Nikki van Driel¹, Amber Q. Mayenburg¹, Diana Lozovagia¹, Eva Roos², Bernadette
437 Schurink², Marianna Bugiani², Ronald E. Bontrop^{1,3}, Jinte Middeldorp¹, Willy M. Bogers¹, Lioe-Fee
438 de Geus-Oei^{5,6}, Jan A.M. Langermans^{1,4}, Marieke A. Stammes^{1‡}, Babs E. Verstrepen^{1‡}, Ernst J.
439 Verschoor^{1‡}

440

441 ¹ Biomedical Primate Research Centre (BPRC), Lange Kleiweg 161, 2288GJ Rijswijk, The
442 Netherlands

443 ² Department of Pathology, Amsterdam UMC, De Boelelaan 1117, 1081HV Amsterdam, The
444 Netherlands

445 ³ Department of Biology, Theoretical Biology and Bioinformatics, Utrecht University, Padualaan
446 8, Utrecht, The Netherlands

447 ⁴ Department Population Health Sciences, Division of Animals in Science and Society, Faculty of
448 Veterinary Medicine, Utrecht University, Yalelaan 1, 3584CL Utrecht, The Netherlands

449 ⁵ Department of Radiology, Leiden University Medical Center, Albinusdreef 2, 2333ZA Leiden,
450 The Netherlands

451 ⁶ Biomedical Photonic Imaging Group, University of Twente, Drienerlolaan 5, 7522ND Enschede,
452 The Netherlands

453

454 † These authors contributed equally

455 ‡ These authors jointly supervised this work

456 *Corresponding author. E-mail: philippens@bprc.nl

457

458

459 **This file includes: Materials and Methods, Table S1**

460

461

462 **MATERIALS AND METHODS**

463

464 **Animals and SARS-CoV-2 exposure**

465 Four cynomolgus macaques (*Macaca fascicularis*) and four Indian-origin rhesus macaques
466 (*Macaca mulatta*) (Table 1) were selected for this study. All macaques were mature, outbred
467 animals, purpose-bred and socially housed at the BPRC. The animals were in good physical health
468 with normal baseline biochemical and hematological values. All were pair-housed with a socially
469 compatible cage-mate. The animals were offered a daily diet consisting of monkey food pellets
470 (Ssniff, Soest, Germany) supplemented with vegetables and fruit. Enrichment was provided daily
471 in the form of pieces of wood, mirrors, food puzzles, and a variety of other homemade or
472 commercially available enrichment products. Drinking water was available *ad libitum* via an
473 automatic system. Animal Care staff provided daily visual health checks before infection, and
474 twice-daily after infection. The animals were monitored for appetite, general behavior, and stool
475 consistency. All possible precautions were taken to ensure the welfare and to avoid any discomfort
476 to the animals. All experimental interventions (intratracheal and intranasal infection, swabs, blood
477 samplings, and PET-CTs) were performed under anesthesia. The research protocol was approved
478 by an independent animal ethics committee (DEC), as well as BPRC's institutional animal welfare
479 body (IvD).

480 On day 0, all animals were exposed to a dose of 10^6 TCID₅₀ of SARS-CoV-2 (strain
481 BetaCOV/BavPat1/2020), diluted in 5 ml phosphate-buffered saline (PBS). The virus was
482 inoculated via a combination of the intratracheal route (4.5 ml) and intranasal route (0.25 ml per
483 nostril). For the histological examination brains from naive control macaques from the same age
484 were obtained from the BPRC biobank, two cynomolgus, and two rhesus macaques.

485

486 **Positron Emission Tomography – Computed Tomography**

487 Positron Emission Tomography (PET)-computed tomography (CT) data were acquired on multiple
488 time points post-infection using a MultiScan Large Field of View Extreme Resolution Research
489 Imager (LFER) 150 PET-CT (Mediso Medical Imaging Systems Ltd., Budapest, Hungary) as
490 described before(40). Animals were fasted overnight (glucose level > 8.5 mmol/l). The animals
491 were sedated with ketamine (10 mg/kg ketamine hydrochloride (Alfasan Nederland BV, Woerden,
492 The Netherlands)) combined with medetomidine hydrochloride (0.05 mg/kg (Sedastart; AST
493 Farma B.V., Oudewater, The Netherlands)) to induce sedation and muscle relaxation, both applied
494 intramuscularly (IM). The animals were positioned head first supine (HFS) with the arms up. The
495 scans were acquired under mechanical ventilation in combination with a forced breathing pattern.
496 For anesthetic maintenance, a minimum alveolar concentration of isoflurane (iso-MAC) of around
497 0,80%-1.00% was used. The body temperature of the animal was maintained by using the Bair
498 Hugger (3M™, St Paul, MN, USA) supplied with 43°C airflow. Typically, around 100 MBq of ¹⁸F-
499 FDG was applied intravenously (GE Healthcare, Leiderdorp, NL). Thirty minutes after injection
500 the plateau in tracer activity uptake is reached, subsequently a PET of 15 minutes was acquired.
501 After the scan, upon return to their home cage, atipamezole hydrochloride (Sedastop, ASTFarma
502 B.V., Oudewater, NL, 5 mg/ml, 0.25 mg/kg) was administrated IM to antagonize medetomidine.
503 Afterward the emission data was iteratively reconstructed (OSEM3D, 8 iterations, and 9 subsets)
504 into a single frame PET image normalized and corrected for attenuation, scatter, and random
505 coincidences using a reference CT and corrected for radioactive decay. The analysis was performed
506 in VivoQuant 4.5 (Invicro, Boston, USA). Based on repeatability parameters for correct
507 interpretation of the results, a standardized uptake value (SUV) ratio was used for robustness(17,
508 40). An increased uptake, and pituitary gland hypermetabolism is defined as a SUV_{mean} ratio above

509 1.5 for the pituitary gland over the surrounding brain in combination with a SUV_{peak} ratio above
510 background levels (>1.0). A group of non-infected control rhesus macaques ($n=6$) were used to
511 calculate average background uptake of ^{18}F -FDG.

512

513 **Brain tissue collection**

514 Five weeks after virus exposure the macaques were euthanized and the brains were collected for
515 further examination. The right hemisphere was used for RT-qPCR analysis and the left hemisphere
516 was fixed in formalin for histology. Fifteen different regions were collected from the right
517 hemisphere for RT-qPCR analysis: 1) part of the pituitary gland, 2) the olfactory bulb, 3) substantia
518 nigra, 4) medulla oblongata, 5) pons, 6) anterior part of the cerebellum, 7) motor cortex medial, 8)
519 sensory cortex, 9) frontal basal cortex, 10) hippocampus, 11) caudate nucleus, 12) hypothalamus,
520 13) globus pallidus, 14) putamen, and 15) thalamus. For the preparation of paraffin-embedded
521 sections of the formalin-fixed left hemisphere, the cerebrum and cerebellum were dissected in 3-4
522 mm parts on the anterior-posterior axis. Pituitary gland and olfactory bulb were also embedded.
523 From each part, sections ($4\ \mu\text{m}$) were prepared for different staining methods.
524 Immunohistochemistry stains were used for T-cells (CD3), B-cells (CD20), activated microglia
525 (Mamu-DR), Lewy bodies (α -synuclein ab), and for SARS-CoV-2. Hematoxyline-eosine (HE)
526 staining was used for general morphology.

527

528 **Viral RNA detection in brain tissue**

529 Brain tissue samples were weighed and placed in gentleMACS M tubes (30 mg in 100 μl PBS) and
530 treated using a gentleMACS Tissue Dissociator (protein01 program)(Miltenyi Biotec B.V., Leiden,
531 The Netherlands). Next, the homogenized tissue was centrifuged, and 100 μl supernatant was used

532 for RNA isolation. Viral RNA was isolated from using a QIAamp Viral RNA Mini kit (Qiagen
533 Benelux BV, Venlo, The Netherlands) following the manufacturer's instructions. Viral RNA was
534 reverse-transcribed to cDNA using a Transcriptor First Strand cDNA Synthesis kit (Roche
535 Diagnostics BV, Almere, The Netherlands). Viral RNA was quantified by RT-qPCR specific for
536 RdRp gene of SARS-CoV-2, as described by Corman *et al.*(41). The lower detection limit of the
537 RT-qPCR was 3.6 viral RNA copies per reaction. Viral sub-genomic RNA was detected essentially
538 as described by Wölfel *et al.*(42). For both assays, RNA standard curves were generated by *in vitro*
539 transcription of the target regions.

540

541 **Tissue preparation for histology**

542 The left hemisphere of the brains, part of the pituitary gland, and one olfactory bulb were fixed in
543 formalin for 24 hours and thereafter stored in buffered PBS. Preserved brains were cryoprotected
544 in 30% w/v sucrose in PBS. The cerebrum was dissected in 12 different parts cut anterior-posterior
545 axis at +10, +8, +5, +1, -3, -6, -8, -11, -14, -18, -22 from Bregma(43), the cerebellum and pons
546 were cut in 4 parts. These part were embedded in paraffin. From the eight brain parts in which viral
547 RNA was detected by RT-qPCR, strips of brain sections were sliced into 12-series of 4 µm sections
548 for different stains. These parts included the frontal cortex, midbrain parts, cerebellum, pituitary
549 gland, and olfactory bulb. Sections were stained with virus antibody staining for virus detection
550 and immunohistochemistry for immune reaction such as T-cell staining (CD3), B-cell staining
551 (CD20), MHC-II cell staining (HLA-DR). Mirror sections were analyzed with a HE staining for
552 brain morphology.

553

554 **Immunohistochemistry**

555 The optimal concentration was determined for each antibody: CD3 (polyclonal rabbit – anti-human
556 CD3 IgG, cat. no. A045201-2, Agilent Technologies), 1:60; CD20 (monoclonal mouse – anti-
557 human CD20 IgG2a, clone L26, cat. no. M075501-2, Agilent Technologies), 1:800; Mamu-DR
558 (monoclonal mouse – anti-human HLA-DR/DQ- IgG1, clone CR3/43, cat. no. M077501-2, Agilent
559 Technologies), 1:150. For antigen retrieval, a steamer was used. Antigen Retrieval solution: IHC-
560 TEK epitope retrieval solution, ready to use (catno IW-1100, IHC world). All incubation steps
561 were at room temperature unless mentioned otherwise. Additionally, hematoxylin was used as a
562 counterstaining in all protocols. After a dehydration sequence, the slides were mounted in Malinol.
563 The counting of cells was performed in a blind matter.

564

565 *CD3 and CD20 staining*

566 The slides were deparaffinized by putting the slides sequentially in xylene, 100% ethanol, 96%
567 ethanol, 70% ethanol, and PBS. Subsequently, an epitope antigen retrieval was executed in a
568 steamer for 1h. After cooling down, the slides were placed in cuvettes (Sequenza cover plate system
569 productnr 36107 Ted Pella inc.). Endogenous peroxidase (PO) activity was blocked by the PO
570 blocking solution from DAKO (S2023) for 15 minutes. After a washing step (PBS with 0.05%
571 Tween) Avidin was added from the DAKO kit (X0590) for 10 minutes. Thereafter, another
572 washing step and biotin was added from the same DAKO kit (10 min) for blocking endogenous
573 biotine. After washing a blocking step was executed for 20 minutes (PBS with 0.1% BSA and 1%
574 normal human serum, NHS). The primary antibody was added (diluted in 0.1% BSA in PBS) and
575 the slices were left overnight at 4°C. After washing a secondary antibody (Rabbit-anti-mouse IgG
576 biotinylated (E0354), Agilent Technologies; 1:200 diluted in PBS + 1% BSA + 1% NHS) was
577 added and, after washing, the slides were incubated with Vectastain ABC-peroxidase (ABC-PO,

578 from Vector Laboratories; PK-4000; diluted 1:100 in PBS) for 30 minutes. After washing, 3,3'-
579 diaminobenzidine (DAB) with 0.02% H₂O₂ was added to visualize the antigen-antibody binding (20
580 min).

581

582 *Mamu-DR staining*

583 The EnVision™ staining kit (Gl2 Double-stain System, Rabbit/Mouse, DAB+/Permanent RED
584 code K5361; Agilent technologies, Dako DK) was used for the immunohistochemical stain of
585 Mamu-DR. The slides were deparaffinized by putting them sequentially in xylene, 100% ethanol,
586 96% ethanol, 70% ethanol, and PBS. Subsequently, an epitope antigen retrieval was executed and
587 the slides were put in a steamer for 1h. The cooled down slides were placed in cuvettes and the
588 endogenous peroxidase activity was blocked by the envision kit. The slides were washed and
589 thereafter a blocking step was used consisting of 1% NHS + 1% BSA + 0.2% triton x100 in PBS
590 for 10 minutes. Subsequently, the primary antibody was added (diluted in 0.1% BSA/PBS) for 30
591 minutes. Thereafter a washing step was implemented and the EnVision™ polymer/HRP (secondary
592 antibody) was added for 10 minutes. Polymer HRP was added for 10 minutes followed by a
593 washing step. Thereafter DAB+ was added for 15 minutes to visualize the antigen-antibody
594 binding.

595

596 *α-Synuclein staining*

597 The slides were deparaffinized by immersing them sequentially in xylene, 100% ethanol, 96%
598 ethanol, 70% ethanol, and PBS. Subsequently, an epitope antigen retrieval was executed by putting
599 the slides for 15 minutes in Formic acid (100%) diluted 1:10 in demineralized water. After 2
600 washing steps in PBS with 0,05% Tween, the slides were placed in cuvettes (Sequenza cover plate

601 system product no. 36107 Ted Pella inc.). Endogenous PO activity was blocked by the PO blocking
602 solution from DAKO (S2023) for 20 minutes. After washing (PBS with 0.05% Tween), avidin was
603 added from the DAKO kit (X0590) for 10 minutes. Then, after another washing step, biotin was
604 added from the same DAKO kit (10 min) for blocking of endogenous biotine. After washing, a
605 blocking step was executed for 30 minutes (PBS with 0.1% BSA and 1% NHS and 0.02% Triton-
606 X100). The primary antibody, α -synuclein clone 4D6 (Biolegend SIG-39720), was added (diluted
607 in 0.1% BSA in PBS) and the slides were left overnight at 4°C. After washing, a secondary antibody
608 (rabbit anti-mouse IgG Biotinylated (E0354), Agilent Technologies; 1:200 diluted in PBS + 1%
609 BSA) was added for 30 minutes and the slides were incubated with Vectastain ABC-PO kit from
610 Vector Laboratories (PK-4000; diluted 1:100 in PBS) for 30 minutes. After a final washing step,
611 DAB with 0.02% H₂O₂ was added to visualize the Antigen-antibody binding (20 min).

612

613 *SARS-CoV-2 staining*

614 The Roche Optiview DAB IHC kit was used in a Ventana Benchmark Ultra (Roche, Basel
615 Switzerland) immunostainer to immunohistochemically stain SARS-CoV-2. Two monoclonal
616 antibodies of ThermoFisher raised to SARS-CoV-2 Nucleocapsid (clone B46F, catno MA1-7404,
617 and E16C, catno. MA1-7403) were validated on formaldehyde-fixed and paraffin-embedded
618 SARS-CoV-2 and mock-infected Vero E6 cells(10), as well as lung tissue sections of human
619 SARS-CoV-2 patients. The clone E16C was superior to B46F and was further used in this study.
620 Antigen retrieval took place with cell conditioning 1 (CC1 , Ventana Medical Systems) (pH 8,5)
621 for 24 minutes at 100°C, 1/5.000 diluted. Thereafter, incubation took place with the primary
622 antibody for 48 minutes at 36°C followed by standard Optiview detection/visualization with DAB
623 and Copper. After immunohistochemical staining, the sections were dehydrated with grades of

624 ethanol and cleared with xylene. All sections were mounted with TissueTek® coverslipping film
 625 (Sakura Finetek Europe B.V., Alphen aan den Rijn, The Netherlands).

626
 627

628 **Table S1: Quantitative PET-CT analysis of the macaque brains**

629 The standardized uptake values (SUVs) of animals C1 and C2 are represented together with the
 630 SUVs of six non-infected control rhesus macaques. Of these animals the average and peak uptake
 631 are determined for the pituitary gland, and the brain minus the pituitary gland. By dividing these
 632 the pituitary gland/brain ratio is calculated. For the SUV_{mean} values above 1.0 are defined as
 633 slightly increased (light grey) and increased (dark grey) when equal or above 1.5. For the SUV_{peak}
 634 values above 1.0 are demarcated as slightly increased and above 1.2 as increased.

| C1 | SUV_{mean} | | | | | SUV_{peak} | | | | |
|------------------------|---------------------------|---------------|---------------|---------------|---------------|---------------------------|---------------|---------------|---------------|---------------|
| <i>Tissue/day</i> | <i>D8/10</i> | <i>D16/17</i> | <i>D22/23</i> | <i>D28/29</i> | <i>D35/36</i> | <i>D8/10</i> | <i>D16/17</i> | <i>D22/23</i> | <i>D28/29</i> | <i>D35/36</i> |
| Pituitary gland | 3.1 | 2.5 | 2.5 | 3.5 | 3.9 | 5.3 | 3.9 | 4.1 | 6.1 | 6.4 |
| Brain | 2.2 | 1.9 | 2.4 | 1.9 | 2.6 | 5.0 | 4.6 | 4.7 | 4.6 | 4.6 |
| Ratio | 1.4 | 1.3 | 1.0 | 1.9 | 1.5 | 1.1 | 0.8 | 0.9 | 1.3 | 1.4 |
| C2 | SUV_{mean} | | | | | SUV_{peak} | | | | |
| <i>Tissue/day</i> | <i>D8/10</i> | <i>D16/17</i> | <i>D22/23</i> | <i>D28/29</i> | <i>D35/36</i> | <i>D8/10</i> | <i>D16/17</i> | <i>D22/23</i> | <i>D28/29</i> | <i>D35/36</i> |
| Pituitary gland | 3.1 | 2.6 | 2.7 | 3.8 | 3.2 | 7.1 | 6.3 | 4.5 | 6.5 | 6.1 |
| Brain | 2.0 | 1.8 | 2.1 | 2.2 | 2.1 | 5.1 | 3.6 | 3.8 | 5.0 | 3.8 |
| Ratio | 1.5 | 1.5 | 1.3 | 1.7 | 1.5 | 1.4 | 1.8 | 1.2 | 1.3 | 1.6 |

635

| Controls | SUVmean | | | | | | SUVpeak | | | | | |
|----------------------------|----------------|-------------|-------------|-------------|-------------|-------------|----------------|-------------|-------------|-------------|-------------|-------------|
| <i>Tissue/ animal</i> | <i>NHP1</i> | <i>NHP2</i> | <i>NHP3</i> | <i>NHP4</i> | <i>NHP5</i> | <i>NHP6</i> | <i>NHP1</i> | <i>NHP2</i> | <i>NHP3</i> | <i>NHP4</i> | <i>NHP5</i> | <i>NHP6</i> |
| Pituitary gland | 2.3 | 2.6 | 2.1 | 2.7 | 1.3 | 1.3 | 3.3 | 3.7 | 2.9 | 3.9 | 1.9 | 1.6 |
| Brain | 2.3 | 2.0 | 1.9 | 1.9 | 1.5 | 1.8 | 5.6 | 6.1 | 4.9 | 3.9 | 3.7 | 3.5 |
| Ratio | 1.0 | 1.3 | 1.1 | 1.4 | 0.9 | 0.7 | 0.6 | 0.6 | 0.6 | 1.0 | 0.5 | 0.5 |

636

637